Nonequilibrium structural changes of a viscoelastic liquid under oscillatory shear: A molecular dynamics study

Hiroshi Komatsugawa* and Shuichi Nosé
Department of Physics, Faculty of Science and Technology, Keio University, 3-14-1 Hiyoshi, Kohoku-ku, Yokohama 223, Japan
(Received 15 May 1995)

The structural changes of a concentrated liquid under an oscillatory shear are investigated by nonequilibrium molecular dynamics simulations. In simulations starting from a liquid, two successive structural changes to layered structures are reproduced, which corresponds well with the experiments by Ackerson and Pusey [Phys. Rev. Lett. **61**, 1033 (1988)]. The nonequilibrium phase diagrams in the space of the frequency, the shear rate, and the number density are also obtained. The nature of the transition from a liquid to ordered structures changes with the frequency. The shear-induced melting is observed at low frequency, while the shear-induced freezing occurs at high frequency. We also find that the behavior of the viscoelastic properties near the shear-induced freezing line is well described by the Maxwell viscoelastic model.

PACS number(s): 82.70.−y, 83.20.Hn, 64.60.−i, 66.20.+d

I. INTRODUCTION

Colloidal suspension systems display a variety of characteristic behavior under shear flows [1–6]. In the experiments under the steady shear flow, Hoffman investigated the structure of the concentrated suspensions at the point where the viscosity exhibits a discontinuous change. He analyzed light diffraction patterns and indicated that an order-disorder transition occurs at this point [2]. Ackerson and Clark investigated the shear-induced melting of the charged colloidal crystal by light scattering and observed that a phase change from the bcc crystal to a disordered structure occurs with increase of the shear rate [4–6].

The behavior under a steady shear has also been investigated extensively in computer simulations [7–13]. One of the typical simulation methods employed in the study of non-Newtonian fluids (i.e., fluids characterized by a shear rate dependent viscosity) is the nonequilibrium molecular dynamics (NEMD). Erpenbeck discovered the string phase in a hard sphere system in a high shear rate region by the NEMD [7]. Particles are aligned along lines parallel to the flow direction and move keeping the sequence in the *string*. The string phase has also been observed in the study with Brownian dynamics simulations [12,13], but has not yet been confirmed in the experiments.

Hess investigated the structural change at solid density in a soft sphere system and observed not only the shear-induced melting of the bcc crystal at an intermediate shear rate but also the shear-induced freezing at a higher shear rate [8]. Stevens *et al.* applied NEMD to a Yukawa system, which is a model for charge-stabilized colloidal suspensions, and studied both the shear-induced melting and ordering under the steady shear, and obtained the nonequilibrium phase diagram in terms of the shear rate and the concentration of the added salt [10,11].

The characteristic structural changes under an oscillatory shear flow were studied experimentally by Ackerson and Pusey [14,15]. In a liquid just below the freezing concentration, structural changes to two layered structures were observed with an increase of the amplitude of the shear oscillation. They considered that the close packed layers are formed perpendicular to the velocity gradient vector and oscillate, synchronizing with the shear in both ordered structures. The intermediate phase exhibited a light scattering pattern corresponding to the fcc crystal when the spectrum was taken in a narrow period near the extrema of the oscillation cycle. As a result, Ackerson and Pusey called this the "fcc" structure, and we will follow this notation. At a higher shear rate, a sixfold scattering pattern was observed. The orientation of the spots was rotated by 30° from that in the "fcc" structure. This structure is called the "layer" structure.

Recently, Yan *et al.* [16] investigated these structural changes with charge-stabilized colloidal particles and obtained the same results as those of Ackerson and Pusey. They also indicated that a series of the structural changes depend on the amplitude and the frequency of oscillation.

We carried out NEMD simulations in a model atomic system interacting via a short range repulsive force and studied the structural changes under the oscillatory shear at density corresponding to the crystalline phase in equilibrium [17]. In simulations starting from a fcc crystal, we obtained two successive structural changes. The structures appearing at high shear rates correspond well to the results in the colloidal suspension system. The stability of the fcc crystal, the "fcc" structure, and the "layer" structure were investigated in a sliding layer model [2,15,17]. The feature of the structures and the nature of the structural changes were explained as follows. Each structure is depicted schematically in Fig. 1. The oscillation of a particle relative to particles in the neighboring close packed layer is indicated by double-headed

*Present address: Department of Material Science, Faculty of Science and Technology, Keio University.

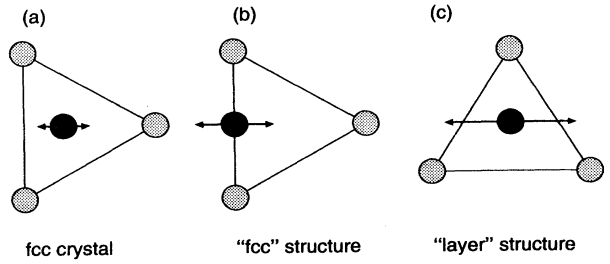

FIG. 1. Three typical structures appearing in the oscillatory shear flow: (a) the fcc crystal, (b) the "fcc" structure, and (c) the "layer" structure. The solid circles and arrows represent the oscillation center and the oscillation of a particle relative to the particles in the neighboring layer.

arrows. In equilibrium or at a small shear rate, a particle oscillates near a stable point situated just above the center of a triangle formed by particles in the neighboring layer [Fig. 1(a)]. If the amplitude of the oscillation is increased, the particle will overlap with a particle in the neighboring layer. The center of the oscillation will shift to the central point of the edge at an intermediate shear rate. A particle visits two centers of the triangle (the lowest energy points) during an oscillation cycle. This is the "fcc" structure [Fig. 1(b)]. If the amplitude is further increased, the overlap occurs once again. In this situation, the direction of the oscillation is changed by 30° and a particle moves along a valley in the neighboring close packed layer. This is the "layer" structure [Fig. 1(c)].

In the present article, we extend our former study and present simulations changing the density and the frequency. In simulations starting from a liquid, we reproduced the structural changes corresponding well with the experiments by Ackerson and Pusey.

The outline of the paper is as follows. In Sec. II, the NEMD method and the model for this study are briefly reviewed. In Sec. III A, results of our simulations starting from a liquid state are presented and compared with the experimental results by Ackerson and Pusey. In Sec. III B, the structural changes are studied in a space of the shear rate, the frequency, and the density, and the nonequilibrium phase diagrams are obtained. In Sec. III C, the viscoelastic properties of the liquid are studied near the transition line between the liquid and the ordered structures.

II. SIMULATION METHOD AND MODEL

Detailed descriptions of the simulation method have been reported previously [17,18]. In this section, we give only a brief description.

We used the Sllod algorithm (so called because of its close connection to the Dolls tensor algorithm) to simulate a system undergoing an oscillatory shear flow. The Sllod method is known to be applicable not only in the linear but also in the nonlinear region of the shear flow when a thermostat is not introduced [19]. Since heat is generated in this type of nonequilibrium simulations, a thermostat should be added to the equations of motion to remove this heat from the system. We employed the Gaussian constraint thermostat assuming a linear velocity profile [20–22]. Equations of motion were integrated with a fifth-order predictor-corrector algorithm. Moreover, to realize the homogeneous shear deformation, the Lees-Edwards periodic boundary condition was imposed [23].

In the NEMD method, the viscosity η is calculated from a ratio of the shear stress P_{xy} and the shear rate $\dot{\gamma}$. We choose the direction of the shear velocity and the velocity gradient along the x and y axes, respectively. Then the shear rate and the viscosity are given by

$$\dot{\gamma} = \frac{\partial v_x}{\partial y} \tag{1}$$

and

$$\eta = -\frac{P_{xy}}{\dot{\gamma}}, \tag{2}$$

where P_{xy} is the xy component of the shear stress and v_x is the flow velocity. With a time dependent shear rate $\dot{\gamma} = \gamma_0 \exp(i\omega_0 t)$, the frequency component of the viscosity $\eta(\omega)$ is given by

$$\eta(\omega) = -\frac{P_{xy}(\omega)}{\gamma_0}\delta(\omega - \omega_0), \tag{3}$$

where $P_{xy}(\omega)$ is the temporal Fourier-Laplace transform of $P_{xy}(t)$ and $\delta(\omega - \omega_0)$ is the Dirac delta function. In our simulations, a sinusoidally changing shear rate $\dot{\gamma}(t) = \gamma_0 \cos(\omega_0 t)$ was applied. The complex shear viscosity $\eta(\omega)$ at $\omega = \omega_0$ was calculated by

$$\begin{aligned}\eta(\omega_0) &= \eta_r(\omega_0) + i\eta_i(\omega_0) \\ &= \frac{-1}{\gamma_0 t}\left(\int_0^t ds \cos(\omega_0 s) P_{xy}(s) ds \right. \\ &\quad \left. + i\int_0^t ds \sin(\omega_0 s) P_{xy}(s) ds\right),\end{aligned} \tag{4}$$

where η_r and η_i are the real and the imaginary parts of $\eta(\omega_0)$.

The colloidal system used in the experiments by Ackerson closely resembles the hard sphere system [15]. The most dominant factor determining the structural changes under the driving shear forces is considered to be the repulsive force due to the overlap of atomic cores [24,25]. It is known that the structural changes under a steady shear do not depend much on the details of interatomic interactions. In all NEMD simulations with hard sphere, soft sphere, and Lennard-Jones systems, qualitatively similar results have been obtained [9]. Therefore, we employed an atomic system interacting via the Weeks-Chandler-Andersen (WCA) potential to simulate the colloidal suspension system,

$$\phi(r) = \begin{cases} 4\epsilon\left\{\left(\frac{\sigma}{r}\right)^{12} - \left(\frac{\sigma}{r}\right)^{6}\right\} + \epsilon & (r < 2^{\frac{1}{6}}\sigma) \\ 0 \quad (r > 2^{\frac{1}{6}}\sigma), \end{cases} \tag{5}$$

which is the Lennard-Jones potential truncated at $r_c = 2^{1/6}\sigma$ and expresses a *short range* repulsive interaction between colloidal particles. This potential has a merit of saving a computational effort since the truncation point is shorter than that of other types of interactions.

Reduced units with the characteristic energy ϵ, the length σ, and the mass of a particle m were introduced. Then, the unit of time is $(m\sigma^2/\epsilon)^{1/2}$ and the unit of temperature is ϵ/k. In this scaled system, a triple point of the WCA potential occurs at $T = 0.75$ and $\rho = 0.96$. In the calculation of $\eta(\omega_0)$, the amplitude of the shear oscillation was increased stepwise with an increment of 0.4. Averages of physical quantities at each γ_0 were taken over the runs of 200 oscillation cycles. Even in the test computation at $\gamma_0 = 0.1$ and $\rho = 0.86$ where the system is dominated by the thermal fluctuation, the error of $\eta(\omega_0)$ was less than 1%. In the nonequilibrium simulations, the choice of the time step δt is important and must also take into account the time scale for the applied shear. In our simulations, δt ranges from $\pi/8000$ to $\pi/2000$, depending on γ_0, ω_0, and ρ.

The initial configuration at $\gamma_0 = 0.0$ was set to the fcc crystal whose (111) vector directs parallel to the velocity gradient vector (y axis). In this orientation, the simulation cell consists of orthorhombic unit cells containing six particles in each of them under the constant volume condition. The system size is given by $N = 6N_xN_yN_z$, where N_x, N_y, and N_z are the number of the cells in the x, y, and z directions. We adopted $N = 504$ ($6 \times 4 \times 3 \times 7$) in the calculation of $\eta(\omega_0)$. We repeated simulations with a 2520 ($6 \times 7 \times 5 \times 12$) particle system at several γ_0 to study the particle configurations more carefully. Moreover, to investigate the system size dependence of the phase change, the simulations with $N = 10\,032$ ($6 \times 11 \times 8 \times 19$) were carried out at $\rho = 0.86$ and $\omega_0 = 20.0$. These three types of system size are chosen so that the simulation cell resembles the cube.

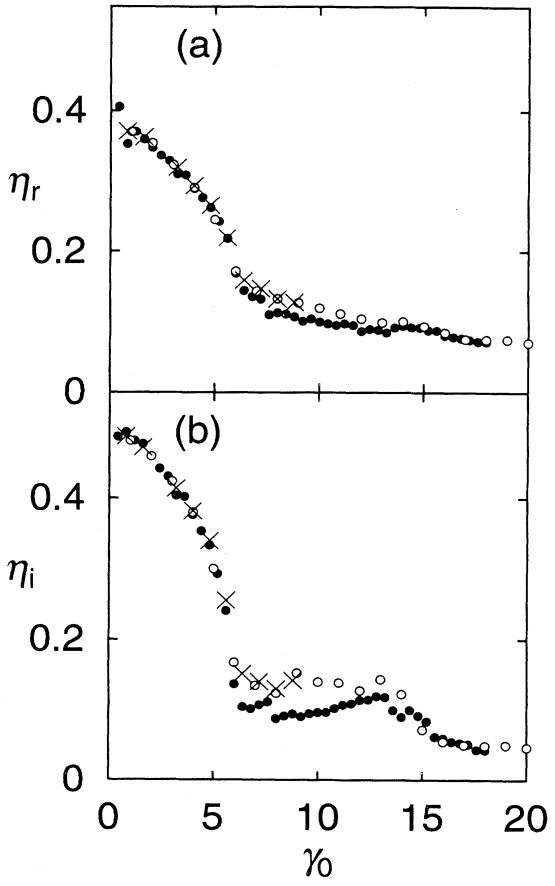

FIG. 2. The γ_0 dependence of the real and the imaginary parts of $\eta(\omega_0)$ at $\rho = 0.86$ and $T = 0.75$. The solid, the open circles, and the crosses indicate the results of $N = 504$, $N = 2520$, and $N = 10\,032$, respectively. The rapid decreases are observed near $\gamma_0 = 5.0$ and $\gamma_0 = 14.0$.

III. RESULTS

A. Structural change at $\rho = 0.86$ and $\omega_0 = 20.0$

In this section, we show the shear rate dependence of the structure at $\rho = 0.86$ and $T = 0.75$ corresponding to a liquid slightly below the triple point density at equilibrium. The frequency of the shear oscillation is $\omega_0 = 20.0$, which corresponds to the inverse of the Maxwell relaxation time. The analysis of the dynamical behavior in the liquid in terms of the Maxwell viscoelastic theory will be presented in Sec. III C.

The γ_0 dependence of the non-Newtonian shear viscosity η_r and η_i is shown in Figs. 2(a) and 2(b). To investigate the system size dependence, simulations with three different system sizes $N = 504$, 2520, and 10 032 were carried out. The solid, the open circles, and the crosses indicate the results obtained in $N = 504$, 2520, and 10 032 systems, respectively. The increment of γ_0 is 0.4 in the case of $N = 504$, 1.0 ($N = 2520$), and 0.8 ($N = 10\,032$). The viscosity curves with different system sizes agree fairly well. We concluded that the system size dependence is not significant in our simulation and further simulations were carried out with $N = 504$ and $N = 2520$ particles. However, we should remark that our simulations were carried out with periodic boundary conditions. If the correlation length of the order is longer than the simulation cell, the local order is strengthened by this. We found that the system size dependence in $N = 504$, 2520, and 10 032 systems is not significant in our study, but simulations with a far larger system might exhibit a deviation from the conclusions obtained in our simulations with relatively small system sizes.

For small γ_0, highly non-Newtonian behavior is observed; the shear viscosity changes with the shear rate. But the system in this small shear region retains a liquid phase. Figure 3(a) shows an atomic configuration projected onto the yz plane at $\gamma_0 = 4.0$. No layered structure is discernible.

At about $\gamma_0 = 5.0$, the η_r and the η_i decrease very sharply. This indicates the structural change from a liquid to an ordered structure. Actually, the snapshot at $\gamma_0 = 8.0$ [Fig. 3(b)] shows a layered structure parallel to the xz plane coexisting with a disordered phase. This disordered phase was also observed even after the simulations were extended to 1000 cycles. Therefore, this

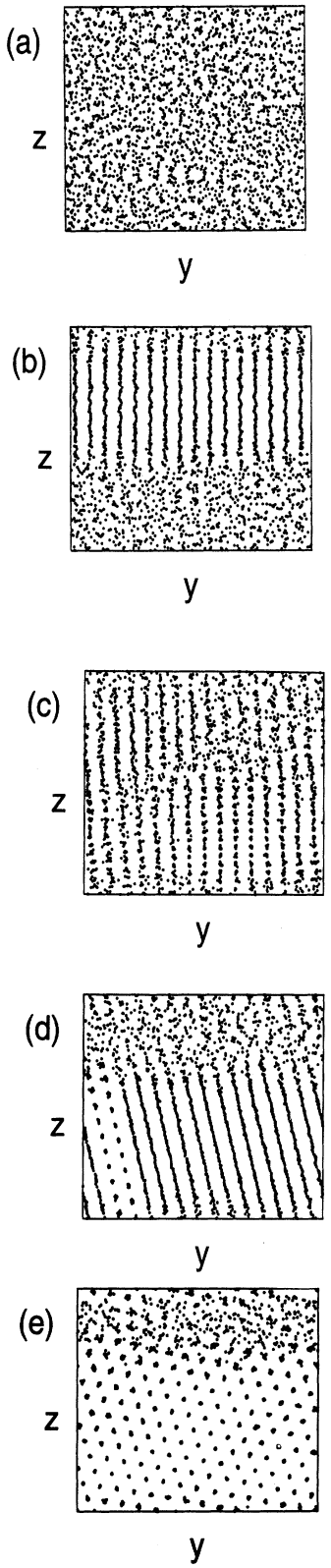

FIG. 3. Particle configurations projected onto the yz planes. The system size N is 2520. (a), (b), (c), and (d) represent the results after the simulation runs of 100 cycles at $\gamma_0 = 4.0$, 8.0, 11.0, and 16.0, respectively. (e) represents the result at the same γ_0 as (d) after 1000 cycles.

coexistence is considered *steady*. The densities of the coexisting phases are 0.7 and 1.0. The boundary between the disordered structure and the layered structure in the coexistence region shows the same orientation as the case of the liquid and the string phase reported in the NEMD simulations under the steady shear flows [9,26]. At $\gamma_0 = 11.0$ [Fig. 3(c)], the ordered structure extends to almost all regions of the simulation cell.

At $\gamma_0 = 14.0$, the viscosity curve takes the second rapid decrease. This indicates that another structural change occurs at this shear rate. At $\gamma_0 = 16.0$ [Fig. 3(d)], a new type of layer is partially produced near the left edge of the simulation cell. We can see distinct spots belonging to the new type of layer whose pattern is different from that shown in Fig. 3(c). Three distinct structures can be recognized in this figure; a disordered phase and two types of layered structures. The coexistence of two types of layered structures is transient, while the coexistence between layered structures and a disordered structure is steady. Actually, the number of layers of the new type increased gradually as the simulation was continued longer. After total runs of 1000 cycles [Fig. 3(e)], the ordered part changed completely to the new layered structure. The disordered phase observed in this shear region disappeared above $\gamma_0 = 18.0$.

The difference between the two layered structures is the orientation of triangular lattices in each layer. We investigated the orientation of the bond vectors to distinguish two layered structures. A bond is defined as a vector connecting a pair of neighboring particles belonging to the same layer perpendicular to the velocity gradient vector (the y axis). We calculated the distribution $f(\theta)$ of the angle θ between the bond vector and the flow direction (the x axis). From Figs. 1(b) and 1(c), we expect that $f(\theta)$ should have peaks at $\theta = 30°, 90°$, and 150° in the "fcc" structure and at $\theta = 0°, 60°, 120°$, and 180° in the "layer" structure. In Fig. 4, the distributions at $\gamma_0 = 12.0$ (solid curve) and $\gamma_0 = 20.0$ (dashed curve) are depicted. We conclude that the system forms the "fcc" structure at $\gamma_0 = 12.0$ and the "layer" structure at

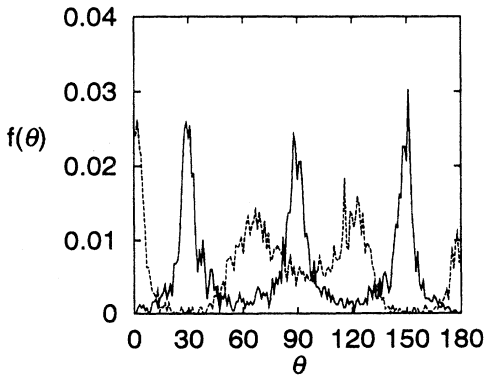

FIG. 4. The distribution of the angle between the bond vector and the flow direction. The solid and the dashed curves represent the results at $\gamma_0 = 12.0$ ("fcc" structure) and $\gamma_0 = 20.0$ ("layer" structure).

$\gamma_0 = 20.0$.

From the shape of the peaks in the angular distribution function, we can estimate the degree of the distortion of the lattice. In the "fcc" structure, the three peaks have roughly the same height and width. Therefore, the triangular arrangement is kept fairly well at a small shear rate. On the other hand, in the "layer" structure, the peaks at $\theta = 0°$ or $180°$ are sharp but the peaks at $\theta = 60°$ and $120°$ are broader than any other peak in Fig. 4. Particles tend to be arranged into a line parallel to the flow but there is some distortion in the relative arrangement of these lines. When the applied shear is increased further, the correlation between neighboring lines becomes weaker. This is a feature similar to the string phase observed in simulations under the steady shear.

B. Nonequilibrium phase diagrams

We repeated simulations similar to those presented in Sec. III A, changing the number density ρ and the frequency ω_0, and obtained nonequilibrium phase diagrams in the space of γ_0, ω_0, and ρ. Simulations were carried out in a 504 particle system. We determined the change of structures by the snapshots of atomic configurations and by the change of the viscosity curve. The diagrams presented in this section are not proper phase diagrams. It is indicated where new structures were observed, even partially, with increase of the amplitude of the shear rate. We did not distinguish between a single phase and coexisting regions because it is very difficult to determine the phase boundary accurately in the coexistence region from the simulations in a small system as reported here.

The phase diagrams in the γ_0-ω_0 space are shown at densities $\rho = 0.86$ [liquid at equilibrium, Fig. 5(a)] and $\rho = 0.96$ [crystal at equilibrium, Fig. 5(b)]. The liquid region means that we did not detect any layered structures. In the high frequency region (roughly $\omega_0 > 4.0$), the equilibrium structure changes successively to the "fcc" and the "layer" structures with increase of γ_0. These structural changes (especially at $\rho = 0.86$) correspond well to those observed in a colloidal system. In the low frequency region ($\omega_0 < 4.0$), the situation changes. In the liquid case ($\rho = 0.86$), the phase of the "fcc" structure disappears and only the transition from the liquid to the "layer" structure is observed. In the crystal case ($\rho = 0.96$), the "fcc" structure melts by further application of the shear and a liquid phase appears. We determined this melting point on the basis of the sharp increase of the viscosity.

The phase diagrams in the γ_0-ρ space (Fig. 6) show clearly the difference of the structural changes in low and high frequency regions. The frequencies are $\omega_0 = 8.0$ in Fig. 6(a) and $\omega_0 = 4.0$ in Fig. 6(b). The density of the triple point in a WCA system is $\rho = 0.96$. At $\omega_0 = 8.0$, shear-induced freezing is observed. The equilibrium liquid at densities above $\rho = 0.85$ changes to the "fcc"

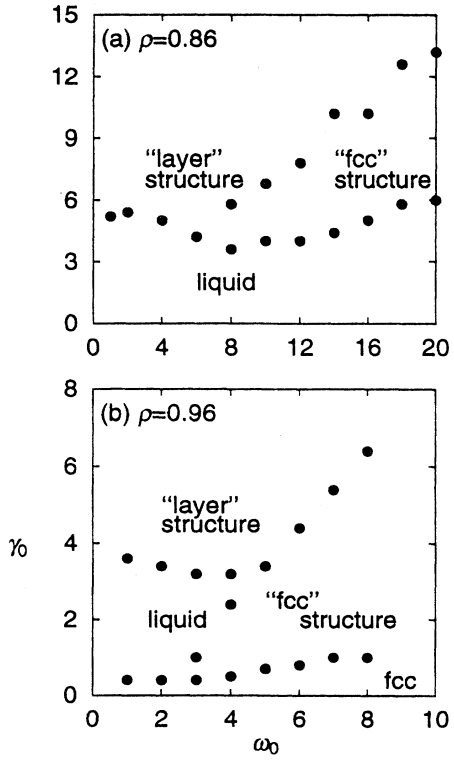

FIG. 5. The nonequilibrium phase diagrams in the space of ω_0 and γ_0. (a) and (b) represent the results at $\rho = 0.86$ (liquid) and $\rho = 0.96$ (crystal), respectively.

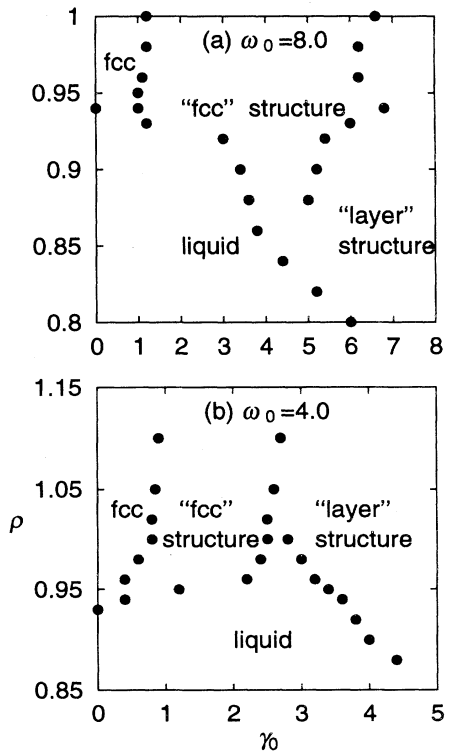

FIG. 6. The nonequilibrium phase diagrams in the space of γ_0 and ρ. (a) and (b) represent the results at $\omega = 8.0$ (high frequency) and $\omega_0 = 4.0$ (low frequency), respectively.

structure with increase of γ_0. On the other hand, at $\omega_0 = 4.0$, there is no density region in which the "fcc" phase emerges from the liquid, and the shear-induced melting occurs in the crystal region below $\rho = 1.0$. The gradient of the phase boundary between the liquid and the "fcc" structure $d\rho/d\gamma_0$ shows these tendencies clearly. At high frequency, it is negative, while at low frequency, it is positive.

The cause of the different behavior of these structural changes is qualitatively explained as follows. In the low frequency region, the time scale determined by the shear oscillation is longer than the Brownian relaxation time. Thus, the motion of particles is dominated by Brownian relaxations. Therefore, the system tends to be random. This mechanism causes the shear-induced melting of the "fcc" structure in the crystal region and the disappearance of the "fcc" structure at a low shear rate in the liquid region. Under the shear with high frequency, the period of the shear oscillation becomes shorter than the relaxation time and each particle is forced to move collectively by the shear before it relaxes to the equilibrium state. Therefore, the system tends to be ordered. This mechanism causes the shear-induced freezing of the liquid.

We can give quantitative support for this interpretation. The two competitive factors can be connected with two typical time scales: the Brownian relaxation time τ and the inverse of the shear rate $1/\dot{\gamma}$ [12]. The Peclet number $P_e = \tau\dot{\gamma}$ is introduced as a ratio of these two competitive factors [27]. In our case, the phase boundary between a liquid and layered structures is situated near $\gamma_0 = 4.0$ throughout the frequency region we investigated. The value $\gamma_0 = 4.0$ corresponds to $P_e \simeq 1.0$ because the relaxation time is estimated to be 0.25 [2.5×10^{-12} (ps)] in the WCA system at $\rho = 0.86$ and $T = 0.75$. At $P_e = 1.0$, the influence of the Brownian force is comparable to that of the shear force. In the experiment by Ackerson, the significant distortion of the equilibrium liquid also occurs at $P_e \simeq 1$ [5,6]. Then, our results for the nonequilibrium phase diagram support the interpretation that the shear-induced structural change relates to the balance between two competitive factors, the Brownian force and the shear force.

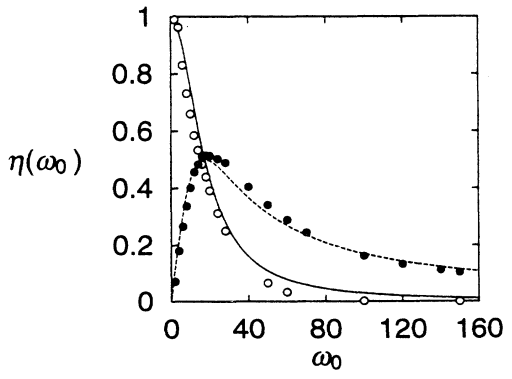

FIG. 7. The frequency dependence of the viscosity at $\gamma_0 = 2.8$. The open and the solid circles represent the real and the imaginary parts, and two lines are the results of Eq. (6) with $\tau = 1/20.0$. Each data is normalized by the values of the real part at $\omega_0 = 0.0$.

C. Viscoelasticity in the liquid region

In the preceding section, we presented the results of the frequency dependence of the structural changes. In this section, we are concerned with the transition between the liquid and the layered structures and analyze the frequency dependence of the viscosity of the liquid near the shear-induced freezing line.

Figure 5(a) shows that, in the simulations starting from the fluid at $\rho = 0.86$, the system retains a liquid phase in the range $0 < \gamma_0 < 3.0$ throughout the frequency region we investigated. The frequency dependence of the viscosity $\eta(\omega_0)$ of the liquid at $\gamma_0 = 2.8$ is shown in Fig. 7 and the $\eta(\omega_0)$ expresses well the viscoelastic behavior of the liquid; the system becomes viscous at low frequency and elastic at high frequency. The open and the solid circles indicate the real and the imaginary parts of the viscosity, $\eta_r(\omega_0)$ and $\eta_i(\omega_0)$, respectively. Each data is normalized by the η_r at $\omega_0 = 0.0$. With increase of the frequency, the η_r decays rapidly, tending to zero as $\omega_0 \to \infty$. This behavior is consistent with a number of experiments and the theoretical results [28–32]. The $\eta_i(\omega_0)$ relates with the energy dissipation due to the viscous properties. The $\eta_i(\omega_0)$ is zero at $\omega_0 = 0.0$ ($t \to \infty$) because the system is steady and there is no dissipation. As the frequency increases, the dissipation induced in the system increases η_i. But in the high frequency region where the elastic properties dominate, the system cannot follow the oscillation, and the dissipation decreases rapidly. Therefore, the $\eta_i(\omega_0)$ has a peak at a critical frequency. The value of ω_0 is roughly estimated to be 20 from Fig. 7.

A simple model for the viscoelasticity in a liquid is the Maxwell model [33]. In this model, a spring (an elastic part) and a dash-pot (a viscous part) are coupled in series, and the total viscoelasticity is expressed as sum of contributions from both parts. The frequency dependent viscosity in this model is expressed by

$$\eta(\omega_0) = \frac{\eta}{1 - i\omega_0\tau}, \tag{6}$$

where τ is the characteristic relaxation time: the inverse of the frequency where the $\eta_i(\omega_0)$ takes the maximum value.

The results of Eq. (6) with $\tau = 1/20$ are depicted in Fig. 7 by lines. They agree fairly well with the NEMD results.

As mentioned in Sec. III B, the nature of the phase transition changes in the range from $\omega_0 = 4.0$ to $\omega_0 = 8.0$; the shear-induced melting occurs at low frequency and the shear-induced freezing is observed at higher frequency. This region is smaller than $1/\tau = 20$, but still in the range of the region where the viscous and the elastic

factors are competing. Therefore, we think that this type of transition between a liquid and ordered structures is determined from the balance between the viscous and the elastic factors.

IV. CONCLUSION

We carried out nonequilibrium molecular dynamics simulations in an atomic system interacting via the WCA repulsive potential undergoing an oscillatory shear flow. In our simulations starting from the liquid state, structural changes closely corresponding with those observed in experiments by Ackerson and Pusey were obtained. We repeated simulations changing the frequency and the density, and obtained the nonequilibrium phase diagram in the space of the frequency, the amplitude of the shear oscillation, and the density. We found that the feature of the structural change between a liquid and ordered structures is different in the low and high frequency regions. At low frequency, the shear-induced melting of the crystalline phase was observed, while at high frequency, the shear-induced freezing of the liquid occurred.

We also found that the frequency dependence of the viscosity in the shear-induced liquid is fairly well described by the Maxwell viscoelastic model. This fact indicates that the dynamical behavior is dominated by the viscous properties related to the Brownian motion at low frequency, and by the elastic properties related to the shear at high frequency. Our result indicates that the structural changes under an oscillatory shear is related to these two competing factors.

ACKNOWLEDGMENTS

We thank J.I. Penman for reading the manuscript carefully. This work is supported by a Grant-in-Aid for Scientific Research on Priority Areas, "Computational Physics as a New Frontier in Condensed Matter Research," from the Ministry of Education, Science, and Culture, Japan. The computations were carried out at Keio University Computer Center and at the Computer Center of the Institute for Molecular Science.

[1] P. Pieranski, Contemp. Phys. **24**, 25 (1983).
[2] R.L. Hoffman, Trans. Soc. Rheol. **16**, 155 (1972).
[3] M. Tomita and T.G.M. van de Ven, J. Colloid Interface Sci. **99**, 374 (1984).
[4] B.J. Ackerson and N.A. Clark, Phys. Rev. Lett. **46**, 123 (1981).
[5] B.J. Ackerson and N.A. Clark, Phys. Rev. A **30**, 906 (1984).
[6] N.A. Clark and B.J. Ackerson, Phys. Rev. Lett. **44**, 1005 (1980).
[7] J.J. Erpenbeck, Phys. Rev. Lett. **52**, 1333 (1984).
[8] S. Hess, Int. J. Thermophys. **6**, 657 (1985).
[9] D.M. Heyes, J. Chem. Soc. Faraday Trans. 2 **82**, 1365 (1986).
[10] M.J. Stevens, M.O. Robbins, and J.F. Belak, Phys. Rev. Lett. **66**, 3004 (1991).
[11] M.J. Stevens and M.O. Robbins, Phys. Rev. E **48**, 3778 (1993).
[12] J.R. Melrose, Mol. Phys. **76**, 635 (1992).
[13] W. Xue and G.S. Grest, Phys. Rev. Lett. **64**, 419 (1990).
[14] B.J. Ackerson and P.N. Pusey, Phys. Rev. Lett. **61**, 1033 (1988).
[15] B.J. Ackerson, J. Rheol. **34**, 553 (1990).
[16] Y.D. Yan, J.K.G. Dhont, C. Smits, and H.N.W. Lekkerkerker, Physica A **202**, 68 (1994).
[17] H. Komatsugawa and S. Nosé, Phys. Rev. E **51**, 5944 (1995).
[18] D.J. Evans and G.P. Morriss, *Statistical Mechanics of Nonequilibrium Liquids* (Academic Press, New York, 1990), Chap. 6.
[19] D.J. Evans and G.P. Morriss, Phys. Rev. A **30**, 1528 (1984).
[20] D.J. Evans, J. Chem. Phys. **78**, 3297 (1983).
[21] W.G. Hoover, A.J.C. Ladd, and B. Moran, Phys. Rev. Lett. **48**, 1818 (1982).
[22] D.J. Evans, W.G. Hoover, B.H. Failor, B. Moran, and A.J.C. Ladd, Phys. Rev. A **28**, 1016 (1983).
[23] A.W. Lees and S.F. Edwards, J. Phys. C **5**, 1921 (1972).
[24] M. Wadati and M. Toda, J. Phys. Soc. Jpn. **32**, 1147 (1972).
[25] S. Hachisu, Y. Kobayashi, and A. Kose, J. Colloid Interface Sci. **42**, 342 (1973).
[26] T. Yamada and S. Nosé, Phys. Rev. A **42**, 6282 (1990).
[27] D.J. Barber and R. Loudon, *An Introduction to the Properties of Condensed Matter* (Cambridge University Press, Cambridge, 1989).
[28] J.C. van der Werff, C.G. de Kruif, C. Blom, and J. Mellema, Phys. Rev. A **39**, 795 (1989).
[29] D. Andrew, R. Jones, B. Leary, and D.V. Boger, J. Colloid Interface Sci. **147**, 479 (1991).
[30] J.D. Landgrebe and S.E. Pratsins, J. Colloid Interface Sci. **139**, 63 (1990).
[31] G.P. Morriss and D.J. Evans, Phys. Rev. A **32**, 2425 (1985).
[32] M.P. Allen and G. Maréchal, Mol. Phys. **57**, 7 (1986).
[33] J.D. Ferry, *Viscoelastic Properties of Polymers*, 3rd ed. (Wiley, New York, 1980).